WrapToR composite truss structures: Measurement and modelling of mechanical response

*Christopher J. Hunt, Yian Zhao, Michael R. Wisnom and Benjamin K.S. Woods

Bristol Composites Institute (ACCIS), Department of Aerospace Engineering, University of Bristol, United Kingdom, BS81TR

**Email: chris.hunt@bristol.ac.uk*

ABSTRACT

Wrapped Tow Reinforced (WrapToR) trusses are ultra-efficient structures that are produced from composite materials using a novel winding process. In this study, a structural model based on the stiffness method is developed for the novel truss configuration to predict the pre-failure mechanical response. To validate the model, the mechanical response of the structures is experimentally investigated to a high level of detail using a series of three-point bend tests. Results of the tests highlight the importance of modelling behaviour of the truss joints due to both internal joint deformations and their effect on load transfer between members. The results also show that the developed model can predict deflections and strains to a reasonable accuracy across a range of truss configurations.

Keywords: Composite trusses; Computational modelling; Mechanical testing; Filament winding

1 Introduction

Lattice structures, such as trusses and space frames, offer high structural efficiencies making them the preferred configurations in a wide range of applications. By grouping material together into localised, discrete elements, they can move material far away from the axis of bending or torsion to create structures with very high stiffness and strength relative to their mass. Also contributing to the historical popularity of these structures is that they can be analysed using relatively simple techniques. Before the advent of computers, the response of a truss could be predicted by applying the assumption that the structure is formed of two-force members that only carry axial loads [1]. The advent of

modern computers led to the development of matrix methods which do not require such assumptions to reduce computational expense. By forming structural problems in a systematic manner that is ideal for computer implementation, the methods made it possible to conduct analyses of large and highly redundant lattice structures that were previously unfeasible to compute by hand [2].

The use of composite materials in lattice structures is an idea that has been gaining popularity in recent years. By producing lattice members from composites, the inherent anisotropy can be taken advantage of by aligning the fibres along the length of the primarily axially loaded members. This synergistic combination of material and geometry can therefore produce highly efficient structures. One earlier example of a composite lattice is the truss concept presented by Schütze [3] which is used commercially in the Zeppelin NT airship. While Schütze's work showed the carbon trusses to weigh roughly half that of a comparable aluminium truss, the manufacturing process requires the assembly of many parts and is, therefore, labour intensive. More modern examples of composite trusses tend to use more advanced manufacturing processes to avoid the need to assemble many parts. The majority of these structures fall into one of two categories: lattice core sandwich panels, such as those seen in [4]–[9], or lattice beams, such as the IsoTruss® [10], [11], Open-Architecture Composite Structures (O-ACS) [12], Advanced Composite Truss (ACT) [13], and other unnamed concepts [14], [15]. Relative to their weight, composite lattice beams have impressive flexural properties, making them highly suitable as lightweight beams members [14] or as compression columns [16], [17].

The patented WrapToR truss concept [18] uses a simple winding process to produce composite lattice beams in which the fibres within each member of the truss are aligned along the length of that member. The novel manufacturing process involves holding premade tubular composite longitudinal members (referred to as chord members) on a rotating mandrel while fibre tow, that has been wetted out with resin, is wound around them. The wetted tow is then cured, forming shear members which are simultaneously co-cured to each other and co-bonded to the underlying chord members. The process can be used to create composite trusses with a variety of shapes and sizes, such as those shown in Figure 1.

Implementation within lattice structures has been highlighted as a means to maximise the benefits of composite materials [19] and the discussed lattice beam concepts have demonstrated highly impressive structural efficiencies. However, to fully unlock the potential of these technologies, the ability to both understand and accurately predict their mechanical response will be needed. This must be achieved through the development and detailed validation of structural models.

Within the literature, several authors have developed structural models to predict lattice beam behaviour under axial, torsional and flexural loading scenarios. While the derivation of analytical expressions for this purpose has been investigated [20], the use of finite element (FE) methods is generally preferred [11], [12], [14], [21]. Although popular, these models are not always stringently validated with authors often comparing to experimental data from only one test configuration. In addition to this, models are generally validated using overall deflection data, meaning the model's ability to predict member stresses or strains is not assessed.

During the preliminary work on the WrapToR truss, a low-fidelity analysis tool based on the stiffness method employing a two force-member assumption was developed [22]. Within the study, this tool was validated by comparing it to experimental deflection data of one high aspect ratio truss subjected to torsional and flexural loads. Later work on the technology looked at improving and automating the WrapToR winding process [23], during which a variety of truss sizes were tested in bending. When comparing these experimental results to the previously developed analysis tool, the model was found to be inaccurate when predicting the flexural response of lower aspect ratio trusses.

Within this study, an improved, higher fidelity truss analysis tool is developed to predict the mechanical response of WrapToR trusses. Two different idealisations of the WrapToR truss geometry are compared which use different methods of representing the truss joints. The model's ability to predict flexural behaviour is validated through testing of five truss configurations under three-point bending. The response is captured to a high level of detail by using a variety of different measurement techniques. This in-depth investigation compares model and experimental data for global truss stiffness, local strains, and local deformations.

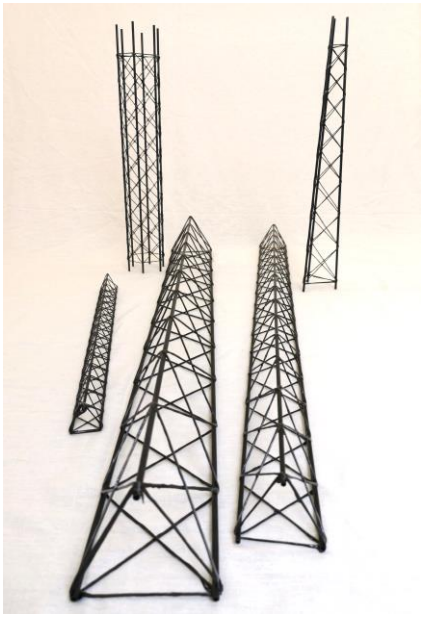

Figure 1: WrapToR trusses.

2 Experiment

To experimentally characterise the mechanical response, five truss configurations were subject to a series of three-point bend tests. During these tests, deformations and member strains were measured using multiple experimental techniques. The experimental work is split into two sections. The first is focused on global truss stiffness and looks at determining the effective flexural rigidities of the truss beams. The second takes a more detailed look at the mechanical response by measuring local deformations and member strains.

2.1 Sample manufacture

For validation of the analysis methods over a range of truss geometries, five configurations were investigated. All configurations have an equilateral triangle cross-section formed of three chord members. For each configuration, three trusses were manufactured using the automated winding machine previously developed and detailed in [23]. Tow feed rate was controlled at 2 m / min resulting in a total winding time of 4 minutes and 20 seconds per truss. Curing of the epoxy shear web matrix was conducted at room temperature. The test samples were manufactured at a length of 1 m

and were tested at multiple spans to investigate any effects of varying aspect ratio. The five configurations are detailed in Table 1 with the related geometric features depicted in Figure 2.

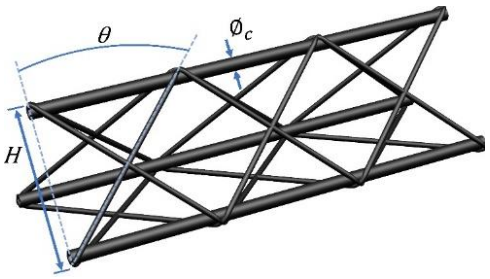

Figure 2: Truss geometry definition.

Table 1: Truss test sample geometric configurations.

Truss configuration ID	Truss height, H (mm)	Chord tube diameter, $\emptyset_c$(mm)	Chord tube wall thickness (mm)	Winding angle, θ (°)	Tow size, N_s	Mass per unit length, (g/m)
H33_1*	33	3	0.5	45.0	24k	33.0
H33_2	33	3	0.5	56.3	24k	31.1
H66_1	66	4	0.5	45.0	24k	41.2
H66_2*	66	4	0.5	45.0	48k	56.2
H99*	99	5	1.0	45.0	96k	102.0

*Configurations tested in both global stiffness and strain tests.

2.2 Global truss stiffness

To determine global bending stiffness behaviour, the five truss configurations were tested in three-point bending using an Intron 8872 universal test machine (UTS) and the custom-built loading rig displayed in Figure 3. The loading rig is built from modular aluminium extrusions allowing the test span to be easily adjusted. Two steel tubes form the end supports and load is introduced to the lower-central truss joints using a 6 mm steel pin. Load was measured with a 5 kN load cell and was applied at a displacement rate of 4 mm / min. Displacement was measured at the two lower central truss joints using laser sensors. To account for any deformations within the rig, displacement of the supports was measured using potentiometers. From the measured displacement, δ, at the centre of truss, the effective flexural rigidity, EI_{eff}, of the truss beam was calculated using the following equation for deflection of a simply supported beam with length L, under loading, P:

$$EI_{eff} = \frac{PL^3}{48\delta} \quad \text{i}$$

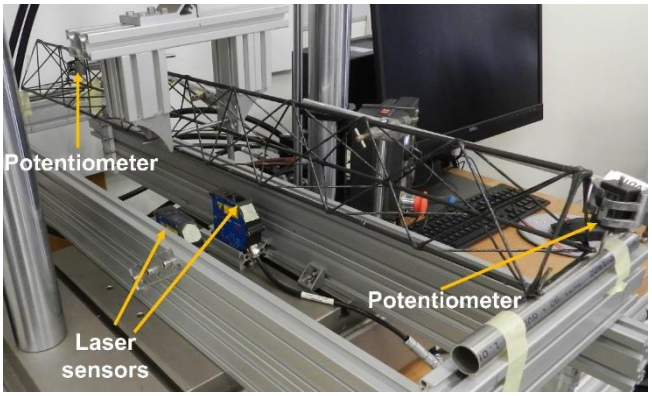

Figure 3: Custom three-point bend test rig.

2.3 Member strains and local deformations

To investigate the mechanical response to a higher level of detail, a second round of testing was conducted in which member strains and local deformations were measured. For these tests, three of the five truss configurations (highlighted in Table 1) were again tested in three-point bending at spans of 792 and 396 mm. Load was applied using hanging weights to provide more space around the structure for positioning of measurement equipment. For configuration H33_1 maximum loads of 10 and 15 kg were applied for 792 and 396 mm span, respectively. All remaining configurations and spans were loaded to 30 kg. For each truss configuration, a variety of instruments were used to measure strains and local deformations, including Digital Image Correlation (DIC), strain gauges, and extensometers.

Figure 4 shows a summary of where strains and local deformations were measured. Detailing of each of these measurements is given within the following sub-sections.

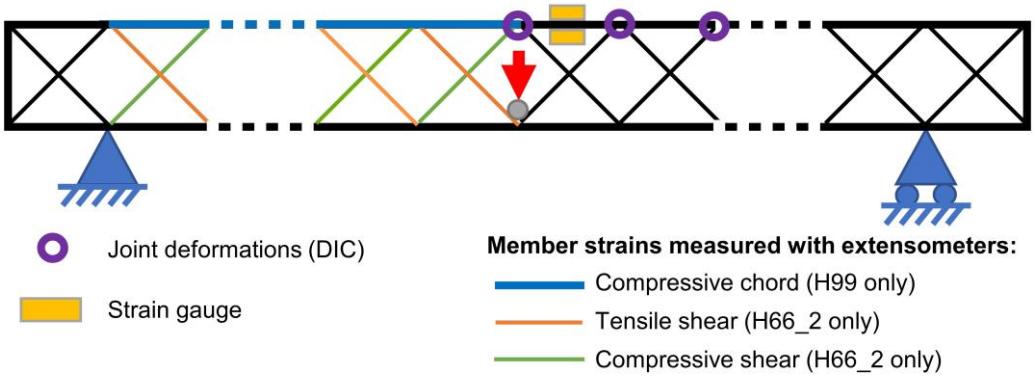

Figure 4: Summary of strain and local deformation measurement methods and locations.

2.3.1 Chord member strain

Two strain gauges were attached to one of the central upper-compressive chord members, as is seen in Figure 5a. This member was chosen because the analysis predicts it to be the most highly strained region of the truss. Strain gauges were placed at the centre span of the member on both the upper and lower surfaces so that bending and axial strain in the member could be determined.

To determine the bending moment distribution within the upper-compressive chord members, the largest truss configuration (H99) was subjected to a series of measurements using clip extensometers (Figure 5b). Again, by taking readings on the top and bottom surfaces of the tube, both the axial and bending strain could be determined. Using the measured bending strain, ε_x, the moment, M_Z, at each measurement point was calculated using the following rearranged form of the engineers bending equation:

$$M_Z = \frac{\varepsilon_x E_x I_z}{y} \qquad \text{ii}$$

where E_x is the longitudinal Young's modulus and y is the section height.

Using this method, the bending moment at one-quarter and three-quarters length of each upper chord member was determined. As loads are only introduced into members at the joints at their ends, the distribution of bending moment across a member will be linear. This means that by measuring the moment at two places within a member, the moment distribution across the length of that member can be determined. By doing this in each upper member along half the truss span and assuming a moment

distribution that is symmetric about the truss centre span, the moment distribution throughout the entire upper compressive pultrusion tube was determined.

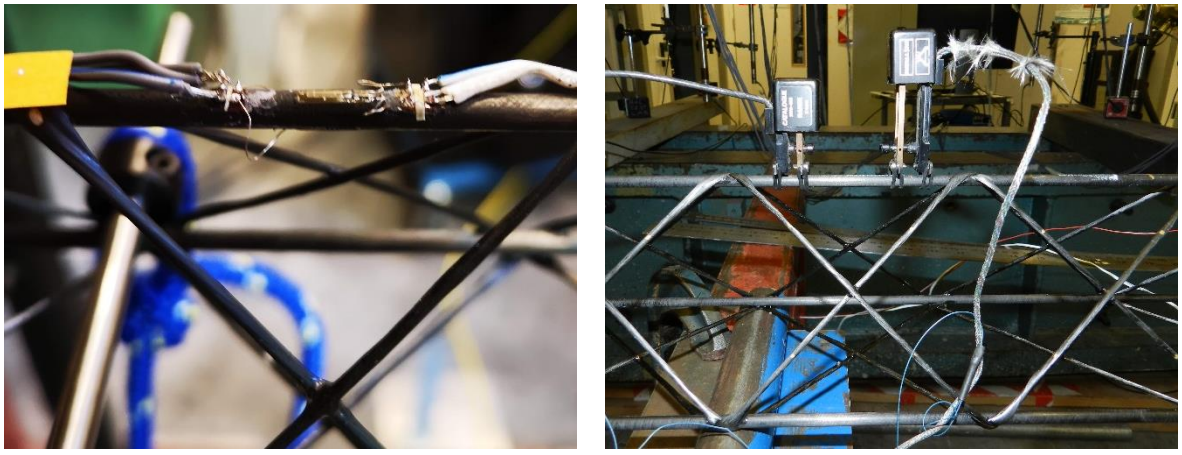

(a) *(b)*

Figure 5: Strain measurements in chord members: a) strain gauge; b) clip extensometers.

2.3.2 Shear member strain

The shear members of the WrapToR truss configuration form a repeating cross pattern. Each cross contains two shear members which are connected at their crossing-point via an epoxy bond that is formed during winding. Using clip extensometers, strain was measured in each shear member above and below this crossing point. Again, to determine axial strain within the member it was necessary to account for bending by measuring the strain on opposing sides of the members. Strains in the shear members were only measured in configuration H66_2 as the smaller configurations were too small to fit the extensometers and the strains in the larger truss were too small to be measured by these devices.

2.3.3 Internal joint deformations

To investigate deformations within the joints that connect the shear and chord members, three joints on each of the trusses were inspected during testing using a 5 MP 3D Digital Image Correlation (DIC) system. Specifically, DIC was used to track the displacement of the joints along the truss length relative to the neighbouring chord members. Those inspected were the upper central joint and the two adjacent upper joints (as seen in

Figure 4). This method was used to get a qualitative interpretation of deflections within the joints.

3 Analysis development

3.1 Matrix structural analysis overview

To predict the structural response of the WrapToR trusses, an analysis tool that uses matrix structural analysis (MSA) was coded in MATLAB®. MSA is a well-established approach to structural analysis and is well documented within the literature. For this reason, only a brief overview of the particular implementation used here is given. For in-depth detailing of MSA methods, the reader is directed to the following textbooks [2], [24], [25].

When using MSA a structure is first geometrically idealised into a series of discrete elements connected at nodes. Force-displacement relationships for each of the elements are then defined based on the element properties. Element geometries and force-displacement relationships are systematically organised using matrix algebra into a form that is convenient for computer implementation. Loads and boundary conditions are then similarly applied. Following this, conditions of equilibrium and compatibility are used to solve the matrix equations to give the element forces and nodal displacements. There are two variants of MSA methods: the force method, and the stiffness method. Within the lesser-used force (or compatibility) method, the element forces are taken as the primary unknowns which are first determined through solving of the compatibility equations. The stiffness (or displacement) method uses the nodal displacements as the primary unknowns which are found by initially solving the equations of equilibrium. Element forces are then determined using compatibility considerations and member force-displacement relationships. Due to its relatively easy implementation in computer codes, the stiffness method is more suitable for large and highly redundant structures which has led to more widespread use [2]. These advantages also make the stiffness method the most appropriate for analysing the WrapToR truss structures and hence, the method is used here.

A key stage within the stiffness method is the formation of the element's stiffness matrix, *k*. Unlike a true pin-jointed truss structure WrapToR trusses contain bonded joints, meaning the members will carry both axial forces and bending moments. Previous work [23] has shown that modelling WrapToR members as truss (or bar) elements that are only capable of carrying axial loads is insufficient to predict deflections within the composite truss structures. To address this, within this study a higher-fidelity model consisting of beam elements was developed and used. The specific stiffness matrix formulation employed here is for shear deformable beam elements, the derivation of which can be found in [24].

3.2 Geometric idealisation

As stated previously the first stage to MSA is the idealisation of the structural geometry into a format that is suitable for computer implementation. When attempting to idealise the WrapToR truss configuration into a series of beam elements an issue is encountered at the truss joints. As the shear member tow is wrapped over the pultruded chord members (and does not run through their centres), placing beam elements along the centre line of the truss members results in an eccentricity where the shear and chord elements do not connect at a node. To deal with this joint eccentricity, two methods of geometric idealisation were investigated. The first, referred to as the concentric model, simply alters the angle of the shear members to remove the eccentricity at the joints, as is depicted in Figure 6a. The change in angle between the physical truss and the geometrically idealised model is typically less than 2 degrees to create concentric joints. The second method does not alter the geometry of the truss members and deals with the eccentricity using an additional beam element at the joint. This method, depicted in Figure 6b, is referred to as the eccentric model. As well as representing the actual truss geometry more closely, this method also has the benefit of being able to model displacements within the joints. The major disadvantage of this method is that representative stiffness properties are needed for the additional joint element. Determining these properties is not trivial and is discussed in the following subsection.

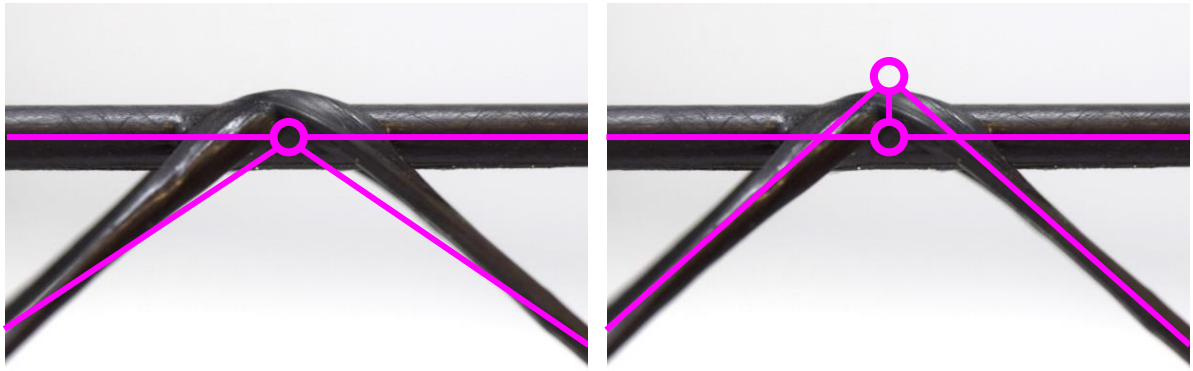

(a) *(b)*

Figure 6: Joint geometric idealisation methods: a) Concentric; b) Eccentric.

3.3 Determining constituent properties

After idealising the structure into a series of elements and nodes, the stiffness properties of the individual elements need to be assigned. For the WrapToR truss configuration, three sets of element stiffness properties need to be defined: chord, shear, and for the eccentric model, joint members. The chord members are formed of carbon-epoxy pultruded tubes purchased from EasyComposites™ and the shear members of Tenax IMS60 carbon fibre tow impregnated with SuperSap™ CLV epoxy resin. To determine Young's modulus, E, the pultruded tubes were tested using ASTM D3916-08 [23] and the impregnated carbon tow using ASTM D4018-17 [24]. For each configuration, a minimum of four samples were tested. Young's moduli from these tests are displayed in Table 2.

The cross-sectional area of the pultrusions was found by measuring the tubes with a micrometre. For the shear members, the area determined using microscopy in the previous study [23] for impregnated 24k tow was used. For the 48k and 96k tow shear members it was then assumed that the areas would be 2 and 4 times larger, respectively. For the material shear modulus, G, a typical value for carbon-epoxy of 4.5 GPa was used [26].

Table 2: Truss constituent properties.

Truss component	Member	Young's modulus (MPa)	Area (mm^2)
CFRP tube: 3 mm	Chord	137.1	3.86
CFRP tube: 4 mm	Chord	136.9	5.42
CFRP tube: 5 mm	Chord	125.1	11.79
Impregnated CFRP 24k tow	Shear	107.8	1.09

In the eccentric model, stiffness properties are also needed for the beam elements representing the joints. This includes the joint elements moduli and cross-sectional area. Accurately determining representative joint stiffness via localised joint testing would be extremely difficult for the given truss configuration. To determine appropriate joint stiffness properties, first, it was assumed that only shear deformations would occur within the joint elements and that axial and bending deformations are negligible. This simplifies the problem and is likely a reasonable assumption given the very low aspect ratio of the joint members. The Young's modulus of the joint elements was therefore increased to a large value (1000GPa) such that changes in E had a negligible effect on the model deformations. A value for the shear stiffness of the elements was then determined by fitting the model results to the experimental data. Through this experimental fit, the shear stiffness of the joint elements that gave the lowest total absolute error across all the test cases was found to be 11,700 N. While it is likely that joint shear stiffness varies between truss configurations, it will later be seen that this constant value provides a reasonable prediction for all the configurations tested.

3.4 MSA verification with commercial FE package

To verify the coded MSA analysis tool, equivalent linear Finite Elements (FE) models for three truss configurations were built in Abaqus using shear deformable beam elements (B32). A single element was used for each truss member. Results comparing the models for a span of 792 mm and a load of 400 N are shown in Table 3. Here it is seen that the MSA model predictions are within 1% of those from FE analysis. The primary advantage of the MATLAB coded MSA tool is that truss geometry is parametrically defined within the code, such that the user can generate new truss configurations and define new analyses by simply specifying the parameters of the truss configuration and the applied loading/boundary conditions. The run time of the MATLAB tool is also very fast. For the truss configurations investigated in this study, a full solution from geometry generation to results output took between 0.17-0.25 seconds on a desktop computer with a 3.4GHz processor and 16GB of RAM. This makes the analysis convenient for future design studies and optimisation.

Table 3: MSA and commercial FE comparison.

Configuration	Load point displacement (mm)			Max element axial force (N)			Min element axial force (N)		
	MSA	FE	% diff.	MSA	FE	% diff.	MSA	FE	% diff.
H33_1	20.62	20.65	-0.14	1435	1436	-0.04	-2943	-2944	-0.04
H66_2	5.286	5.296	-0.20	665.5	665.6	-0.02	-1411	-1412	-0.02
H99_1	-2.284	-2.304	-0.88	417.9	418.2	-0.06	-917.4	-918.1	-0.07

4 Results & Discussion

4.1 Global stiffness

In Figure 7 the experimentally determined effective flexural rigidities of each truss configuration are compared with predictions from the concentric and eccentric models. For each truss configuration, experimentally determined effective flexural rigidity is seen to increase with span; a trend that also features in the model results. This is due to the relative contributions of shear and bending deflections to the overall measured deflection at varying spans. At shorter spans, the contribution of shear deflection is larger and therefore lower effective flexural rigidities are observed. As the span increases, shear deformations become less significant and the bending rigidity approaches a constant value.

Also plotted in Figure 7 are flexural rigidity , EI, predictions determined using parallel axis theorem assuming contributions from the chord members only. This method has been used by some authors to estimate IsoTruss® flexural rigidity for global buckling predictions [27], [28]. In all test cases, parallel axis theorem is seen to overpredict EI. However, for the smaller section beams (Figure 7a and b) the model and experimental results appear to approach the predictions of parallel axis theorem at larger spans. In fact, model results approach predictions from parallel axis theorem for all configurations if the beam aspect ratio is sufficiently high. When running the eccentric model for a high beam aspect ratio (span divided by height) of 120, the determined EI is found to be within 1% of that predicted by parallel axis theorem for all five configurations. Again, this can be explained by the relative contributions of bending and shear deformations. At higher beam aspect ratios, bending deflections dominate meaning parallel axis theorem can provide reasonable predictions.

When comparing experimental results of the different test configurations, Figure 7 demonstrates how the WrapToR trusses take advantage of the non-linear scaling laws of stiffness to achieve impressive stiffness increases with only relatively small mass penalties. When comparing configurations H33_1 and H66_1 at the largest span, a 25% increase in mass corresponds to a 200% increase in stiffness. This is possible because the truss configuration can move material further away from its neutral axis using relatively small amounts of additional material.

One issue faced during testing was that it was difficult to precisely level the trusses so that all four support points and both load points were in contact with the testing rig. This was particularly challenging in the configurations with larger shear members as the truss joints protruded further. This gives some reasoning as to why there is a reasonable variation in measured stiffnesses between the three different specimens of each configuration, as shown by the plotted error bars. Manufacturing inconsistencies between samples is also likely to be a contributing factor, particularly the variation of resin content within the shear member tow. It should be noted here that due to the high stiffness of the structures the measured displacements were very small. For example, the H99 truss at 396 mm span had a maximum displacement of 1.34 mm at 405 N. At these low displacements small measurement errors can have a large effect on the calculated stiffness.

Figure 7 also displays the predictions from the MSA models. When comparing the two geometric idealisation methods, large differences in predictive capabilities are observed. For the concentric model, the average absolute error is 102% with a maximum error of 313%. Comparing this to the eccentric model, which has an average absolute error of 6% and a maximum of 17%, shows that the eccentric model produces significantly more accurate predictions of the global truss stiffness. The key difference between the models is the insertion of an additional element at each joint. The results in Figure 7, therefore, indicate that the detailed joint mechanics have a significant effect on overall truss deflections. The first possible reason for this is due to displacements within the joint. The epoxy joints are the only elements within the trusses that do not have fibres directly aligned with their primary loading direction meaning that although they are small relative to the truss members, their deflections

may be significant. The second possible reason is that the eccentricity of the joint affects how forces are transferred between members. These reasons are investigated and discussed further in the following experimental sections.

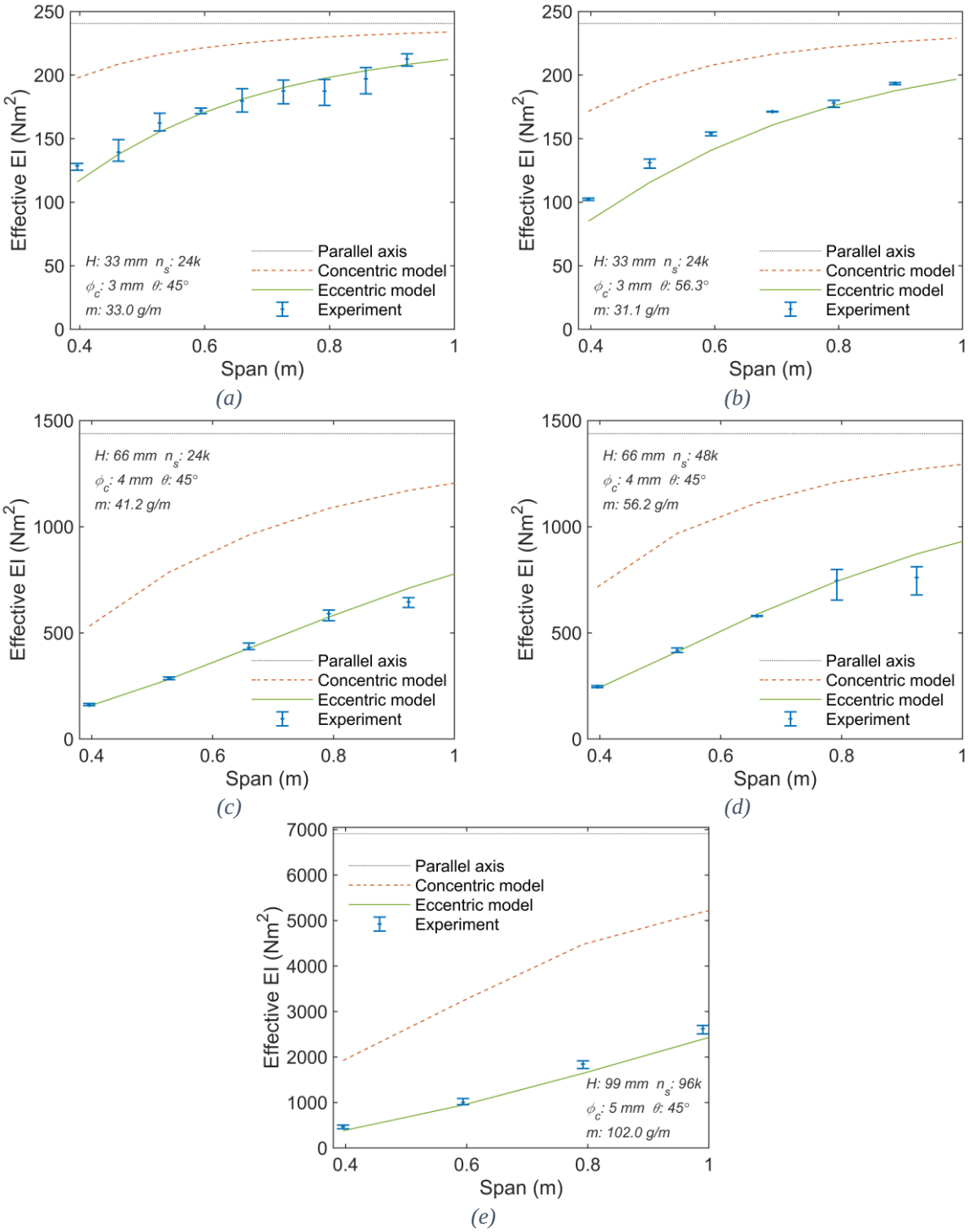

Figure 7: Flexural rigidities of truss configurations at varying spans: a) H33_1; b) H33_2; c) H66_1; d) H66_2; e) H99. (Error bars denote the experimental range of 3 values)

As was stated previously in Section 3.3, the value of shear stiffness used for the joint elements in the eccentric model was found empirically via an experimental fit that minimised the average model error over all the configurations. Each configuration has different joint geometries and therefore the resulting shear stiffness would be expected to vary between configurations. However, it is seen in Figure 7 that using the determined value of 11,700 N provides a reasonable fit across all the configurations tested. To further study this, a sensitivity analysis was conducted to investigate the effect of varying the joint element shear stiffness on the overall average error of the eccentric model predictions. The sensitivity analysis results seen in Figure 8 show that around the determined optimal value, the model error is insensitive to changes in joint element shear stiffness. A 25% increase or decrease in the shear stiffness from the optimal value results in only a 1% change in the average model error. This likely explains why the shear value used provides reasonable predictions over the variety of truss configurations tested.

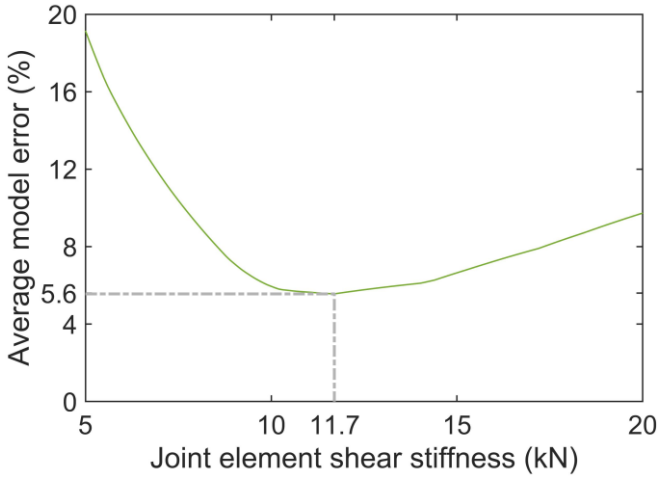

Figure 8: Average error of eccentric model at varying joint elements shear stiffness.

4.2 Member strains and local deformations

4.2.1 Chord member strains

Within Figure 9 readings from strain gauges are compared to the model predictions for each truss configuration. Readings were taken on the upper and lower surfaces of the central upper-compressive chord member on each truss. These two readings are plotted as the minimum and maximum values.

The average of the two readings gives the axial strain within the member which is also plotted within the graph. The difference between the axial and the minimum and maximum values represents the bending strain within the member. The results show that the two geometric idealisation methods are effective at predicting axial strains within the members, with the average error for the concentric method being 4% and the eccentric method being 5%. While both the models predict axial strain effectively, they produce substantially different predictions of the bending strain within the central upper chord member. The results in Figure 9 show the concentric model underpredicts the magnitude of the bending strain for all configurations and spans tested. Meanwhile, the eccentric model provides a more accurate prediction of the bending strain.

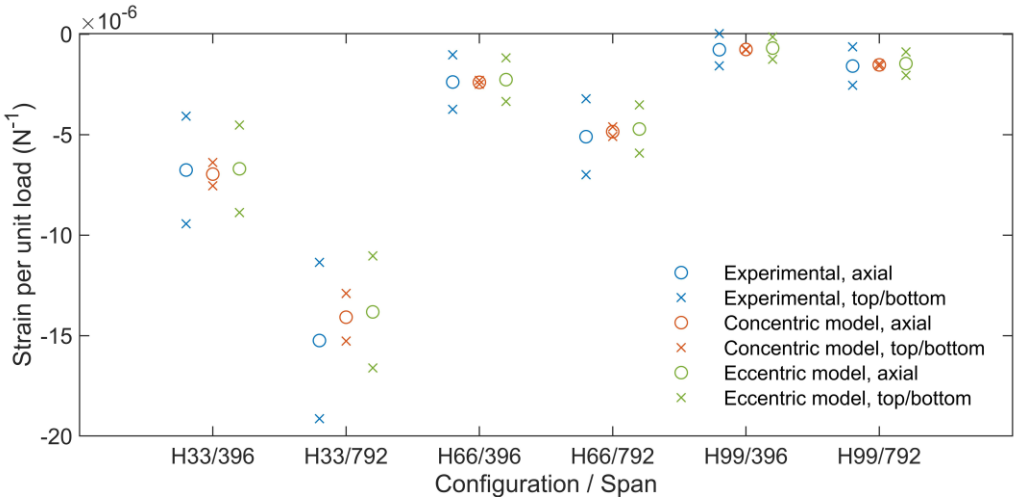

Figure 9: Strain gauge results compared to predictions from MSA.

To further asses the abilities of the models to predict member bending behaviour within the trusses, predicted bending moments in the upper compressive chord members are compared to experimental readings in Figure 10. As stated in Section 2.3.1, the experimental data points shown here were determined using clip extensometers positioned at two points per member. By assuming a linear distribution, the bending moment across the length of the member is then found by interpolating and extrapolating the data from the measured points. The results show that bending moments predicted by the eccentric model (Figure 10b) are larger and show closer agreement with the experimental results than the concentric model (Figure 10a). Within the eccentric model, forces are transferred from the

shear to the chord elements via a joint element. The length of this joint element creates a moment arm meaning that axial forces within the shear elements impart a moment on the chord elements at the joints. This explains why large step changes in bending moment are observed at the joints. This phenomenon has also been witnessed by Tousignant and Packer [29], where it was seen that modelling of the joint eccentricity was necessary for capturing bending moments within the chord members of hollow section metallic trusses.

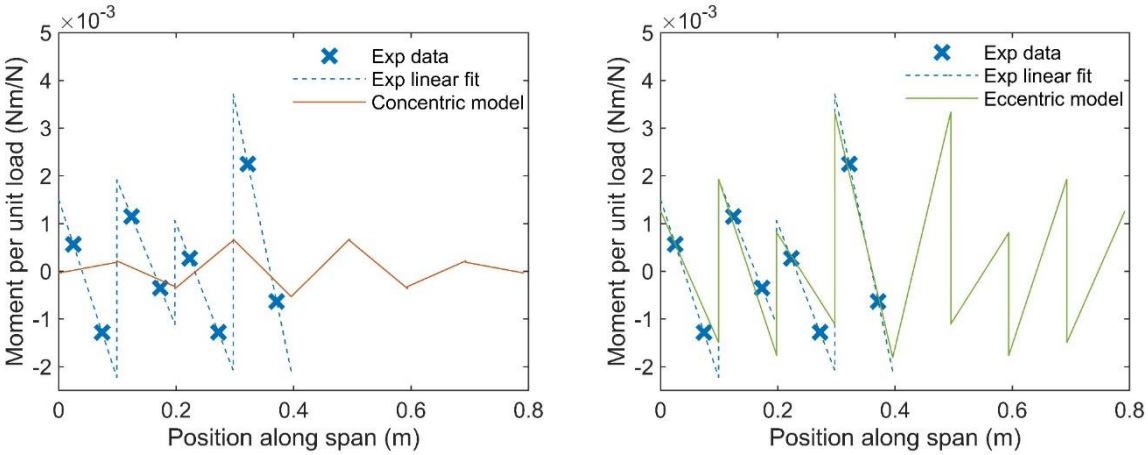

Figure 10:Bending moment distribution in upper chord members of H99 at 792 mm span. Experimental data and: a) concentric model; b) eccentric model.

4.2.2 Shear member strains

Shear member axial strains determined using clip extensometers are displayed for the tensile and compressive shear members in Figure 11. The experimental range plotted for each shear member represents the range of two readings: one above the shear member cross-over point and one below. To determine the axial strain within the member it was necessary to account for bending strain by averaging extensometer readings taken on opposite sides of the shear members.

For the tensile shear member results in Figure 11, both models provide similar predictions of axial strain. Compared to the average of the experimental results, the models perform well for the first two bays (less than 3% error) but show some error for the latter three (15-21% error). For the compressive members, a larger difference between the two models is observed. A larger error is also observed when comparing the models to the compressive experimental data where the concentric model gives

an average error of 26% and the eccentric model 20%. This suggests again that as was seen for the chord members in Section 4.2.1, the two models provide similar levels of accuracy when predicting axial strains. The results here potentially show inaccuracies in the models' ability to predict axial strain within the shear members. However, it should be noted here that acquiring the strain readings in these members was a difficult task. Firstly, the members are very small and have an uneven surface. This made it difficult to take readings on directly opposite sides of each member. Secondly, the strains being measured were very small and were close to the lower limit of what can be measured with the clip extensometers.

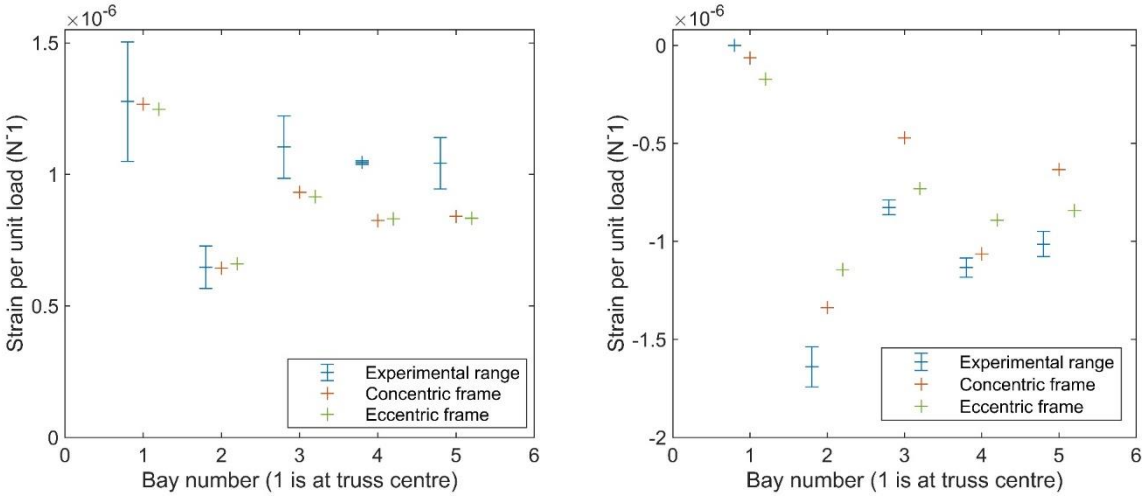

Figure 11: Axial strain per unit load in the shear members for configuration H66_2 at 792 mm span. a) Tensile members; b) Compressive members. (Error bars denote the experimental range of two readings)

4.2.3 Local joint deformations

Tracking the local displacements of the three upper joints (positioning detailed in

Figure 4) revealed an interesting phenomenon. Figure 12 shows the displacements transverse to the loading direction of a single joint measured using DIC. The specific joint shown is adjacent to the upper central joint on configuration H99 tested at a span of 792 mm. Within Figure 12 the joint displays larger displacements transverse to the loading direction than the neighbouring chord members. This shows that the joint deforms at a local level. For the image in Figure 12, the load point is to the left (in the negative x-direction) of the joint and the loading direction is in the image z-axis.

When the truss is loaded the shear members on the left of the image are in tension and on the right are in compression. This means a resultant force acting towards the centre of the truss is experienced which causes the joint to be pulled towards the truss centre. Transverse joint deflections relative to the chord members were not witnessed at the central upper joint. This would be expected as for the central joint all connected shear members are in tension meaning no resultant transverse force is exerted on the joint. This phenomenon potentially provides reasoning as to why the concentric model fails to predict global displacements correctly, as without deformable joint elements these local displacements cannot be captured. It should be noted here that while only results for configuration H99 are displayed, this was observed in all configurations.

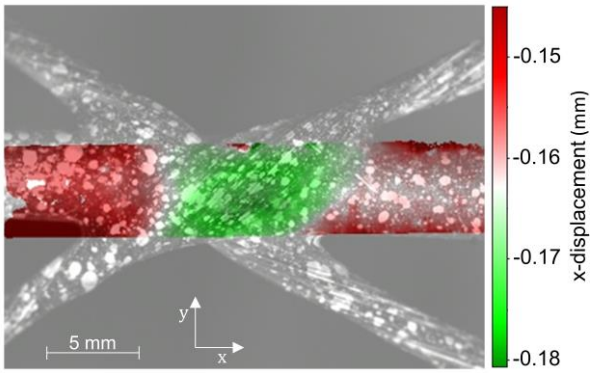

Figure 12: Displacements in truss joint for configuration H99 at 792 mm span and 294 N loading.

4.3 Relevance of findings to other technologies

While this study is focused on the WrapToR technology, findings related to the importance of modelling joints are likely to be useful when developing structural models for other composite lattice technologies. This is particularly the case for structures that feature eccentric member connections such as Open-Architecture Composite Structures (O-ACS) [12], Advanced Composite Truss (ACT) [13], and other unnamed concepts [14], [15]. Indeed recent work published by Shen et al. [21], highlighted the importance of joint torsional stiffness when modelling O-ACS. The IsoTruss® technology creates a concentric connection between members by interweaving the longitudinal and helical member tows. While results in Figure 7 suggest a concentric configuration should provide

higher flexural rigidity, results of a study by Hansen and Jensen [30] have shown interweaving of the member tow to be detrimental to member strength due to the resulting curved fibre paths.

5 Conclusions and future work

This paper details the development of a structural model for WrapToR composite trusses. A thorough experimental investigation used a range of measurement techniques to observe their flexural response to a high level of detail. These experimental findings are then compared with predictions from two analysis models that use different geometric idealisations of the truss geometry. Results highlight the importance of modelling effects of the truss joints using dedicated joint elements when predicting truss deformations and member bending strains. The investigation provided two reasons for the need to include joint members. Firstly, the eccentricity at the joint has a significant effect on how forces are transferred between members, specifically that axial forces within the shear members impart bending moments in the adjacent chord members. Secondly, investigation using digital image correlation (DIC) showed that displacements occur within the joints themselves. Without the use of joint elements within the model, neither of these physical effects can be captured. When modelling the truss without using joint elements the model significantly overpredicts truss stiffness and underpredicts member bending strains. These results therefore clearly show that physical effects associated with the joints have a significant effect on the overall mechanical response.

The work shows that when incorporating joint elements, the model can predict the detailed mechanical response to a reasonable level of accuracy. This includes predicting global bending behaviour, local deflections, and member strains. This is demonstrated across a range of truss configurations with varying section size, member dimensions and truss aspect ratios. While being able to predict stiffness is useful for design purposes, demonstrating the ability to predict strains is ultimately a step towards modelling failure. The next step therefore will focus on incorporating and validating failure criterion within the model. Following this, the model will be implemented within an

optimisation framework to allow efficient component design in which truss geometry is optimised to minimise mass.

6 Acknowledgements

This work was supported by the Engineering and Physical Sciences Research Council through the EPSRC Centre for Doctoral Training in Advanced Composites for Innovation and Science [grant number EP/G036772/1].

7 Data statement

All the raw data used within this study is available for download at the University of Bristol data repository, data.bris, at https://doi.org/10.5523/bris.uj53x9tqzu8x2eiywhnee3up1.

8 References

[1] S. Krenk and J. Høgsberg, *Statics and Mechanics of Structures*. Dordrecht: Springer Netherlands, 2013.

[2] A. Kassimali, *Matrix Analysis of Structures*, Second. Global Engineering: Christopher M. Shortt, 2000.

[3] R. Schütze, "Lightweight carbon fibre rods and truss structures," *Mater. Des.*, vol. 18, pp. 231–238, 1997, doi: 10.1016/S0261-3069(97)00056-3.

[4] M. Eichenhofer, J. C. H. Wong, and P. Ermanni, "Continuous lattice fabrication of ultra-lightweight composite structures," *Addit. Manuf.*, vol. 18, pp. 48–57, Dec. 2017, doi: 10.1016/j.addma.2017.08.013.

[5] T. George, V. S. Deshpande, K. Sharp, and H. N. G. Wadley, "Hybrid core carbon fiber composite sandwich panels: Fabrication and mechanical response," *Compos. Struct.*, vol. 108, no. 1, pp. 696–710, 2014, doi: 10.1016/j.compstruct.2013.10.002.

[6] B.-C. Lee, K.-W. Lee, J.-H. Byun, and K.-J. Kang, "The compressive response of new composite truss cores," *Compos. Part B Eng.*, vol. 43, no. 2, pp. 317–324, Mar. 2012, doi: 10.1016/j.compositesb.2011.08.048.

[7] K. Finnegan, G. Kooistra, H. N. G. Wadley, and V. S. Deshpande, "The compressive response of carbon fiber composite pyramidal truss sandwich cores," *Int. J. Mater. Res.*, vol. 98, no. 12, pp. 1264–1272, Dec. 2007, doi: 10.3139/146.101594.

[8] J. Xiong *et al.*, "Bending behavior of lightweight sandwich-walled shells with pyramidal truss cores," *Compos. Struct.*, vol. 116, no. 1, pp. 793–804, Sep. 2014, doi: 10.1016/j.compstruct.2014.06.006.

[9] J. Xiong, L. Ma, S. Pan, L. Wu, J. Papadopoulos, and A. Vaziri, "Shear and bending performance of carbon fiber composite sandwich panels with pyramidal truss cores," *Acta Mater.*, vol. 60, no. 4, pp. 1455–1466, Feb. 2012, doi: 10.1016/J.ACTAMAT.2011.11.028.

[10] L. R. Francom and D. W. Jensen, “Three-dimensional iso-tross structure,” 13-Jul-1999.

[11] D. Jensen, M. Redford, and L. Francom, “On the structural efficiency of three-dimensional isogrid designs,” *37th Struct. Struct. Dyn. Mater. Conf.*, pp. 1704–1710, 1996, doi: doi:10.2514/6.1996-1508.

[12] A. Gurley, D. Beale, R. Broughton, and D. Branscomb, “The Design of Optimal Lattice Structures Manufactured by Maypole Braiding,” *J. Mech. Des.*, vol. 137, no. 10, p. 101401, 2015, doi: 10.1115/1.4031122.

[13] Q. P. McAllister, J. Senne, and A. Romanyszyn, “Development of a Continuous Advanced Composite Truss Printing System,” in *3rd AIAA Spacecraft Structures Conference*, 2016, no. January, pp. 1–18, doi: 10.2514/6.2016-1705.

[14] S. Ju, D. Z. Jiang, R. A. Shenoi, and J. Y. Xiao, “Flexural properties of lightweight FRP composite truss structures,” *J. Compos. Mater.*, vol. 45, no. 19, pp. 1921–1930, 2011, doi: 10.1177/0021998311410237.

[15] R. P. Hoyt, J. Cushing, J. Slostad, and G. Jimmerson, “TRUSSELATOR: On-Orbit Fabrication of High-Performance Composite Truss Structures,” in *AIAA SPACE 2014 Conference and Exposition*, 2014, no. August, pp. 1–10, doi: 10.2514/6.2014-4337.

[16] M. E. Rackliffe, D. W. Jensen, and W. K. Lucas, “Local and global buckling of ultra-lightweight IsoTruss® structures,” *Compos. Sci. Technol.*, vol. 66, no. 2, pp. 283–288, Feb. 2006, doi: 10.1016/j.compscitech.2005.04.038.

[17] C. Lai, J. Wang, C. Liu, H. Fan, B. Xu, and K. Wu, “A flexible tooling and local consolidation process to manufacture 1D lattice truss composite structure,” *Compos. Sci. Technol.*, vol. 113, pp. 63–70, 2015, doi: 10.1016/j.compscitech.2015.03.018.

[18] B. Woods, B. Otto Berry, and V. Bohdan Stavnychyi, “Continuous Wound Composite Truss Structures,” US2013/0291709, 2013.

[19] K. D. Potter, M. R. Wisnom, M. V Lowson, and R. D. Adams, “Innovative approaches to composite structures,” *Aeronaut. J.*, vol. 102, pp. 107–111, 1998, doi: https://doi.org/10.1017/S0001924000065659.

[20] T. Weaver and D. W. Jensen, “Mechanical characterization of a graphite/epoxy IsoTruss,” *Jorunal Aerosp. Eng.*, vol. 13, no. January, pp. 23–35, 2000, doi: 10.1061/(ASCE)0893-1321(2000)13:1(23).

[21] Y. Shen and D. J. Branscomb, “A general approach to fast prototype the topology of braided structures,” *Int. J. Eng. Sci.*, 2018, doi: 10.1016/j.ijengsci.2018.06.006.

[22] B. K. S. Woods, I. Hill, and M. I. Friswell, “Ultra-efficient wound composite truss structures,” *Compos. Part A Appl. Sci. Manuf.*, vol. 90, pp. 111–124, Nov. 2016, doi: 10.1016/j.compositesa.2016.06.022.

[23] C. J. Hunt, M. R. Wisnom, and B. K. S. Woods, “WrapToR composite truss structures: Improved process and structural efficiency,” *Compos. Struct.*, vol. 230, p. 111467, Dec. 2019, doi: 10.1016/j.compstruct.2019.111467.

[24] J. S. Przemieniecki, *Theory of Matrix Structural Analysis*. McGraw-Hill Inc.,US, 1968.

[25] W. McGuire, R. H. Gallagher, and R. D. Ziemain, *Matrix Structural Analysis*, Second. Wiley, 1999.

[26] D. B. Miracle and S. L. Donaldson, Eds., *ASM Handbook Volume 21: Composites*. ASM Internationl, 2001.

[27] M. E. Rackliffe, D. W. Jensen, and W. K. Lucas, “Local and global buckling of ultra-

lightweight IsoTruss® structures," *Compos. Sci. Technol.*, vol. 66, no. 2, pp. 283–288, Feb. 2006, doi: 10.1016/j.compscitech.2005.04.038.

[28] Q. Sui, C. Lai, and H. Fan, "Buckling failure modes of one-dimensional lattice truss composite structures," *Proc. Inst. Mech. Eng. Part G J. Aerosp. Eng.*, vol. 232, no. 13, pp. 2565–2583, Oct. 2018, doi: 10.1177/0954410017716194.

[29] K. Tousignant and J. A. Packer, "Analysis of Rectangular Hollow Section Trusses," *Can. J. Civ. Eng.*, vol. 175, no. February 2018, pp. 160–175, 2018, doi: 10.1139/cjce-2018-0105.

[30] S. M. Hansen and D. W. Jensen, "Influence of Consolidation and Interweaving on Compression Behavior of IsoTruss Structures," *Des. Nat. II*, 2004.